An Oblique Cutting Based Mechanical Model For Insertion Torque of Dental Implant

Luli Li
Shandong University
Song Zhang (zhangsong@sdu.edu.cn)
Shandong University https://orcid.org/0000-0001-5565-2290
Quhao Li
Shandong University
Cuirong Bian
Shandong University
Airong Zhang
Shandong University

Original Article

Keywords: Insertion torque, Mechanical model, Oblique cutting, Dental implant

Posted Date: December 1st, 2020

DOI: https://doi.org/10.21203/rs.3.rs-116066/v1

Title page

An oblique cutting based mechanical model for insertion torque of dental implant

Lu-Li Li, received her master degree from *Shandong University, China*, in 2019. Her research interests include dental implant and bone mechanics.
E-mail: sdbolll@163.com

Song Zhang, received his Ph. D. degree from *Shandong University, China*, in 2004. He is currently a professor and doctoral supervisor at *School of Mechanical Engineering, Shandong University*, China. His research fields are fundamental mechanism of high-efficiency cutting and machined surface integrity, biomechanics, and so on.

Tel: +86-531-88392746; E-mail: zhangsong@sdu.edu.cn

Qu-Hao Li, received his PhD degree from *Dalian University of Technology, China*, in 2017. He is currently a lecture at *School of Mechanical Engineering, Shandong University, China*. He His research interests include computational solid mechanics, numerical simulation.

E-mail: quhaoli@sdu.edu.cn

Cui-Rong Bian, received her M.M. degree from S*handong University, China*, in 2004. She is currently a Professor and a chief physician at Department of Prosthodontics, Qilu Hospital of Shandong University. Her research fields are fixed porcelain repair, reconstruction of maxillofacial bone defects, implant surgery and design, design and fabrication of denture, and so on.
E-mail: cuirong_b88@163.com

Ai-Rong Zhang, received her PhD degree from *Shandong University, China*, in 2020. Her research interests include bone mechanics, dental implant and numerical simulation of bone tissue.
E-mail: zhangar_ll@163.com

Corresponding author：Song Zhang　E-mail：zhangsong@sdu.edu.cn

ORIGINAL ARTICLE

An oblique cutting based mechanical model for insertion torque of dental implant

Lu-Li Li[1, 2] • Song Zhang[1, 2] • Qu-Hao Li[1, 2] • Cui-Rong Bian[3] • Ai-Rong Zhang[1, 2]

Received June xx, 201x; revised February xx, 201x; accepted March xx, 201x

Abstract: The insertion torque of a dental implant is an important indicator for the primary stability of dental implants. Thus, the preoperative prediction for the insertion torque is crucial to improve the success rate of implantation surgery. In this present research, an alternative method for prediction of implant torque was proposed. First, the mechanical model for the insertion torque was established based on oblique cutting process. In the proposed mechanical model, three factors, including bone quality, implant geometry and surgical methods were considered by defined bone-quality coefficients, chip load and insertion speeds, respectively. Then, the defined bone-quality coefficients for cancellous bone with the computed tomography (CT) value of 235~245, 345~355 and 415~425 Hu were obtained by a series of insertion experiments of IS and ITI implants. Finally, the insertion experiments of DIO implants were carried out to verify the accuracy of developed model. The predicted insertion torques calculated by the mechanical model were compared with that acquired by insertion experiments, which were agreed match with the relative error less than 15%. This method reduces the time consumption on establishing the fitting equations for different implants and enhance the predicted accuracy by considering the effects of implants' geometries and surgical methods.

Keywords: Insertion torque • Mechanical model • Oblique cutting • Dental implant

1 Introduction

Implant dentures have been one of the most popular options for teeth loss in the last decade [1]. After the implant socket is prepared by a series of processes such as drilling, reaming and tapping, an implant is inserted in alveolar bone with a certain torque, named the insertion torque. Many clinical data have shown that 30~70 N·cm is a reasonable range of insertion torque for the great primary stability of implants, and therefore it has been accepted to evaluate surgical success [2–4]. Although the reasonable range of insertion torque are determined by many factors such as shape and diameter of implants [5–6], loading condition [7], or age, gender and height of patients [8–9], it would not be discussed in the present research. As the insertion torque could not be obtained until the implant was fully inserted, if the implant was fully inserted and the insertion torque was not in the reasonable range, the implantation surgery would most likely fail and the patient have to endure a second surgery. Therefore, to improve success rate and avoid the second surgery, preoperative prediction for the insertion torque of implants have been the focus in clinical.

In current clinical researches, computed tomography (CT) value has been used to evaluate the condition of bone quality and proved positively correlated with the insertion torque [10,11]. In addition, the effects of implant geometries [12] and surgical methods [13–14] on insertion torque have been realized. For example, the larger insertion torque will be obtained by a conical [15], large-diameter implant [16] or a small-diameter implant socket [17,18]. As there are no quantitative models to describe the effects of implant geometry and surgical methods on insertion torques, many researchers focus on the empirical formulas fitted by CT value to predict the insertion torque [19–21]. Although the accuracy of these fitting formulas is mostly more than 80%, however, they would not work once the implant or the surgery method was changed. Moreover, it is a time and

✉ Song Zhang
zhangsong@sdu.edu.cn

[1] School of Mechanical Engineering, Shandong University, Jinan 250061, PR China

[2] Key Laboratory of High-efficiency and Clean Mechanical Manufacture (Shandong University), Ministry of Education, PR China

[3] Department of Prosthodontics, Qilu Hospital of Shandong University, Jinan 250012, PR China

money consuming project to establish fitted formulas for all implants and surgical methods.

In this present research, an alternative method was provided by establishing the mechanical model for the insertion torque of a dental implant. In the proposed mechanical model, three factors, including bone quality, implant geometry and surgical methods were considered by defined bone-quality coefficients, chip load and insertion speeds, respectively. Two kinds of bone-quality coefficients for different forming methods were obtained for bone with the CT value of 235~245, 345~355 and 415~425 Hu by a series of insertion experiments of IS and ITI implants, respectively. And the accuracy of developed model was verified by DIO implants with the relative error less than 15%.

2 A mechanical model based on oblique cutting theory

The insertion processes of dental implants involves two forming methods, i.e., the thread-cutting process [22] for implants with cutting edges and the thread-forming process for implants without cutting edges [23]. In this section, the implant typed DIO SFR5010 (DIO Innovation Health Care, Busan City, Korea) with 4 cutting edges in the apical part and continuous threads in the tail part were selected to establish the mechanical model for insertion torque.

2.1 Forming process of matching threads

Figure 1 describes the geometry of DIO SFR5010 and its insertion process. In the insertion process, each thread would process a layer of bone material as the implant fed into the predrilled implant socket. When the implant was inserted into the implant socket, the matching threads were firstly cut by the cutting edges in the apical part. This is the thread-cutting process with physical displacement and chip separate of bone material [24]. Until the apical part was fully inserted into the implant socket, the processed mating threads were further formed by continuous threads in the tail part. This is the thread-forming process with only physical displacement but no chip separate of bone material. Meanwhile, the thread-cutting process still continuous and the torque were increasing. Until the implant was fully inserted into the implant socket, the torque reached peak point—this is the insertion torque discussed in this research.

In this process, the shape of matching threads experienced both thread-cutting and thread-forming process were defined by the last contacted continuous thread while that of threads only experienced the thread-cutting process were defined by the last contacted cut edge. In order to detail the shape of matching thread, DIO SFR5010 was cut into 12 thin slices with one thread involved in and in the apical part, each slice was further separated into 4 cutting elements by 4 cutting edges. Two coordinate systems were defined. The global coordinate system $\{\boldsymbol{C}:OXYZ\}$ was attached to the implant with the Z-axis along the rotation axis. The cutting element coordinate system $\{\boldsymbol{c}:ox_iy_iz_i\}$ was attached to each cutting element with the x-axis paralleling the helical path, where i indicates the ith thread.

Supposing the starting point as M(b,0,0) in $\{\boldsymbol{C}:OXYZ\}$, the helical path of threads can be expressed as follows:

$$g(P,\theta)=\begin{cases}x(P,\theta)=(P\theta/2\pi tan\beta+b+h_d)\cdot\cos\theta\\ y(P,\theta)=(P\theta/2\pi tan\beta+b+h_d)\cdot\sin\theta\\ z(P,\theta)=P\theta/2\pi\end{cases} \tag{1}$$

where, x, y, z are the point coordinates of the helical path, θ is the angle position of the helical path, b, h_d, P and β is initial radius, tooth height, pitch and taper angle of DIO SFR5010, respectively. Particularly, in the tail part, there is β=0.

The radial distance r_i from the Z-axis to outer geometry of ith thread can be expressed as:

$$r_i=\sqrt{x(P,\theta_i)^2+y(P,\theta_i)^2} \tag{2}$$

The radial engagement h_i of ith cutting element can be calculated as follows:

$$h_i=\begin{cases}r_k-H_k/2=r(P,\theta_k)-H_k/2 & i=k\\ r_i(P,\theta_i)-r_i(P,\theta_i-\theta_{i-1}) & i\neq k\end{cases} \tag{3}$$

where, r_k is the first contacted cutting element, H_i is the diameter of the implant socket connecting ith cutting element.

The inclination angle of threads γ can be calculated as follows:

$$\gamma=\pi/2+\xi-\lambda=\pi/2+\arctan(P/2\pi r_i)-\lambda \tag{4}$$

where, ξ and λ is the thread lead angle and the flute helix angle, respectively.

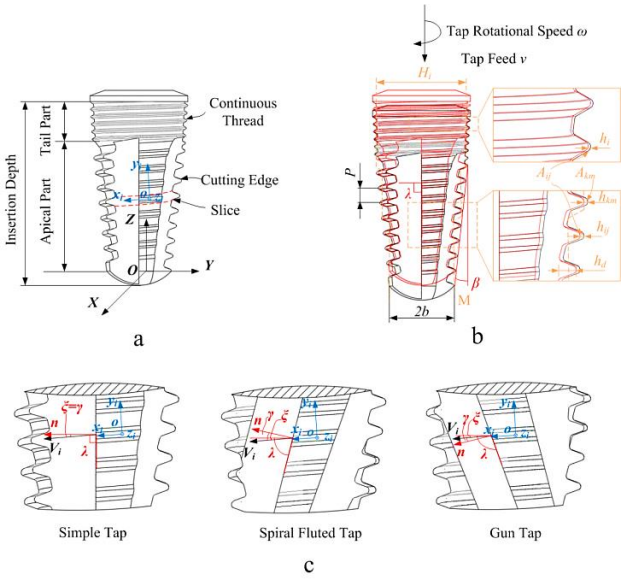

Figure 1 DIO SFR5010 and its insertion process: (a) the geometry of DIO SFR5010 and two coordinate systems, (b) geometric parameters of DIO SFR5010 and the insertion process: the initial position was in red and the position of one rotation cycle was in black, (c) the relationship of angle parameters γ, ξ and λ.

2.2 Force–chip load relationship

Before the forces during the insertion process were discussed, three assumptions were made as follows: (i) each cutting element sustained normal and friction forces, and all forces are applied on the centroid of the respective faces; (ii) the effects of elastic recovery for the prediction of insertion torque were ignored; (iii) insertion torques generated by one thread remained constant throughout the whole insertion process.

According to assumptions, the forces applied on all cutting elements can be composed of the normal force F_n and the friction force F_f as follows [25]:

$$F_n = K_n A \tag{5}$$

$$F_f = K_f A \tag{6}$$

where, A is chip load, which equal to the unformed chip area and depend on the implant geometry, K_n and K_f are specific energies, which are related to the tool geometry and work conditions as follows [26]:

$$\ln K_n = a_0 + a_1 \ln h + a_2 \ln V + a_3 \ln h \ln V \tag{7}$$

$$\ln K_f = b_0 + b_1 \ln h + b_2 \ln V + b_3 \ln h \ln V \tag{8}$$

where, V is the insertion speed, h is the radial engagement of each cutting element, a_0~a_3 and b_0~b_3 are the specific energy coefficients, which are dependent on materials of cutting tool (i.e., implant) and the workpiece (i.e., cancellous bone). As most of implants' material are titanium or titanium-alloys, therefore, the a_0~a_3 and b_0~b_3 were only determined by bone quality and defined as bone-quality coefficients.

Considering the normal force F_n and the friction force F_f are different during thread-cutting and thread-forming processes, they would be discussed in sections 2.2.1 and 2.2.2, respectively.

2.2.1 Forces in thread-cutting process

As shown in Figure 2, the oblique cutting model [27,28] was established based on coordinate system $\{\boldsymbol{c}:ox_iy_iz_i\}$ to define the forces on each elements during thread-cutting process. Two planes, the normal and chip-flow plane, were introduced. The normal plane was defined by the x_i-axis and z_i-axis and the chip-flow plane was coincident with the rake surface of cut edges. In normal plane, the normal force F_{cni} was defined perpendicular to the rake surface. In chip-flow plane, the friction force F_{cfi} was defined collinear with chip-flow orientation [29]. Meanwhile, the chip-flow angle i was defined equal to the inclination angle γ based on the Stabler's rule.

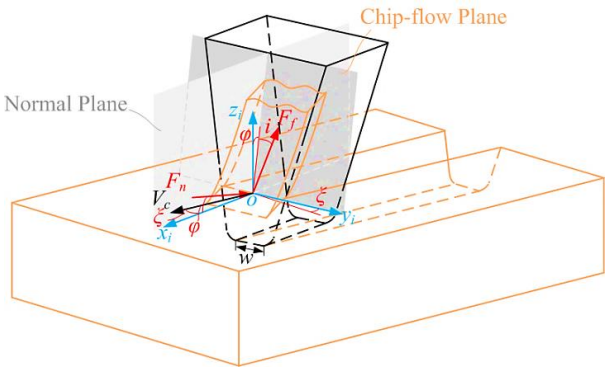

Figure 2 The oblique cutting process

According to Equations (5) and (6), F_{cni} and F_{cfi} can be expressed as follows:

$$F_{cni} = K_{cn} A_{ci} \tag{9}$$

$$F_{cfi} = K_{cf} A_{ci} \tag{10}$$

where, A_{ci} are the chip load of the ith cutting element, K_{cn} and K_{cf}, the specific energies in thread-cutting process. According to Equations (7) and (8), they can be calculated as:

$$\ln K_{cn} = a_0 + a_1 \ln h_i + a_2 \ln V_i + a_3 \ln h_i \ln V_i \tag{11}$$

$$\ln K_{cf} = b_0 + b_1 \ln h_i + b_2 \ln V_i + b_3 \ln h_i \ln V_i \tag{12}$$

where, a_0~a_3 and b_0~b_3 are the bone-quality coefficients during thread-cutting processes, which would be further determined by insertion experiments.

The chip load A_{ci} can be calculated as follows:

$$A_{ci} = h_i\left(w_i + 2h_i\tan\alpha_1 + 2h_i\tan\alpha_2\right) \tag{13}$$

where, w is the tooth top width of ith cutting element, the radial engagement h_i can be calculated according to Equation (3) as:

$$h_i = \begin{cases} r_k - H_k/2 = r(P,\theta_k) - H_k/2 & i = k \\ r_i(P,\theta_i) - r_i(P,\theta_i - 2\pi/N_t) & i \neq k \end{cases} \tag{14}$$

Where, N_t is the number of cutting edges. There is $N_t = 4$ in DIO SFR5010.

By decomposing F_{cni} and F_{cfi} into the three axes of $\{\boldsymbol{c}{:}ox_iy_iz_i\}$, three axial forces F_{x_i}, F_{y_i} and F_{z_i} can be obtained as follows:

$$\begin{pmatrix} F_{x_i} \\ F_{y_i} \\ F_{z_i} \end{pmatrix} = \begin{pmatrix} \cos\varphi \\ 0 \\ -\sin\varphi \end{pmatrix} F_{cni} + \begin{pmatrix} -\sin\varphi \\ \sin\gamma \\ \cos\gamma\cos\varphi \end{pmatrix} F_{cfi} \tag{15}$$

Then, the thrust force F_{thr_i} and tangential force F_{tan_i} of each cutting element and the total insertion torque M can be calculated as Equations (16–18), respectively.

$$F_{tan_i} = F_{x_i}\cos\xi + F_{y_i}\sin\xi \tag{16}$$

$$F_{tan_i} = F_{x_i}\cos\xi + F_{y_i}\sin\xi \tag{17}$$

$$M = \sum_{i=1}^{n} F_{tan_i}\cdot r_i \tag{18}$$

2.2.2 Forces in thread-forming process

In order to define the forces during thread-forming process, six faces named S_1~S_6 were introduced as shown in Figure 3. The ridge would be formed as the plastic deformation and flow of bone material during the insertion process.

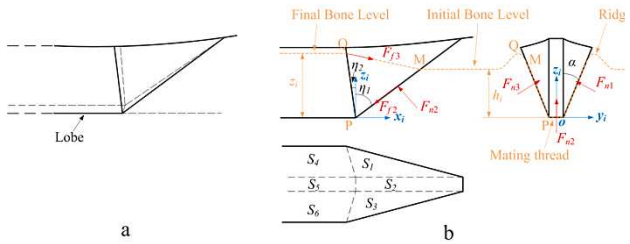

Figure 3 A typical form tap tooth: (a) the schematic diagram of form tap tooth; (b) three views of ith tooth.

As same as the thread-cutting process, the normal forces F_{ni} were defined proportional to the contact areas, and the friction forces F_{fi} were defined collinear with chip-flow orientation [30]. F_{fn_i} and F_{ff_i} can be expressed as follows:

$$F_{fni} = K_{fn}A_{fi} \tag{19}$$

$$F_{ffi} = K_{ff}A_{fi} \tag{20}$$

where, K_{fn} and K_{ff} were the specific energies during the thread-forming process. According to the Equations (7) and (8), they could be calculated as:

$$\ln K_{fn} = c_0 + c_1\ln h_i + c_2\ln V_i + c_3\ln h_i\ln V_i \tag{21}$$

$$\ln K_{ff} = d_0 + d_1\ln h_i + d_2\ln V_i + d_3\ln h_i\ln V_i \tag{22}$$

where, c_0~c_3 and d_0~d_3 are the bone-quality coefficients in the thread-forming process and they would be further determined by insertion experiments.

The chip load A_{fi} can be calculated as follows:

$$A_{fi} = \begin{cases} S_1 = S_3 = \left|\overrightarrow{PQ}\times\overrightarrow{PM}/2\right| = h_i\cdot z_i\cdot y(\eta)/2 \\ S_2 = w\cdot h_i/\cos\eta_1 \end{cases} \tag{23}$$

where, $y(\eta)$ is expressed as:

$$y(\eta) = \sqrt{(\tan\alpha)^2 + (\tan\eta_1\tan\alpha)^2 + (\tan\eta_1 + \tan\eta_2)^2} \tag{24}$$

where, h_i is the radial engagement of ith thread and it was given as Equation (3), α is the thread angle, η_1 and η_2 is the incident angle and lobe-relief angle of threads, respectively, z_i is the z coordinate of point Q and it is given as follows:

$$z_i = \sum_{n=1}^{i} h_i = r_i(P,\theta_i) - r_k(P_k,\theta_k) \tag{25}$$

where, r_k is the first-contacting thread.

By decomposing F_{fni} and F_{ffi} of the ith thread into three axis of $\{\boldsymbol{c}{:}ox_iy_iz_i\}$, three axial forces can be obtained as follows:

$$\begin{pmatrix} F_{x_i} \\ F_{y_i} \\ F_{z_i} \end{pmatrix} = \begin{pmatrix} -\cos\eta_1 \\ 0 \\ \sin\eta_1 \end{pmatrix} F_{fni} + \begin{pmatrix} \sin\eta_1 \\ 0 \\ \cos\eta_1 \end{pmatrix} F_{ffi} \tag{26}$$

Then, the thrust force F_{thr_i} and tangential force F_{tan_i} of each cutting element and the total insertion torque M can be calculated as follows:

$$F_{tan_i} = F_{x_i}\cos\xi + F_{y_i}\sin\xi \tag{27}$$

$$F_{thr_i} = F_{y_i}\cos\xi - F_{x_i}\sin\xi \tag{28}$$

$$M = \sum_{i=1}^{n} F_{tani}\cdot r_i \tag{29}$$

According to Equations (15–18) and (26–29), it could be observed that the insertion torque was related to the normal and friction force and further determined by *a*) bone-quality coefficients, *b*) insertion speed V, c) radial

engagement h_i and d) chip load A. These give a good explanation for the effects of bone quality, surgical methods and the implant geometry, respectively. When the implant and the surgical method were selected, h_i, A and V were determined. The only consideration is the bone-quality coefficients, which were given in the section 3.

3 Determination of bone-quality coefficient and validation of mechanical model

To define the bone-quality coefficients, more than 80 bone blocks with the size of 25 × 25 ×40 mm^3 were cut from the epiphysis areas of four bovine femurs with different age, weight and gender as shown in Figure 4. The mean CT value of bone material within 1 mm around the predicted implant socket for each bone block were recorded by Planmeca ProMax 3D Mid CT (Planmeca UK Limited, London, UK. scanning time: 13.929 s, tube voltage: 90 kV tube current: 10mA). According to recorded CT value, 36 bone blocks were selected and further classified into 3 groups with CT value of 235~245, 345~355, and 415~425 HU, respectively.

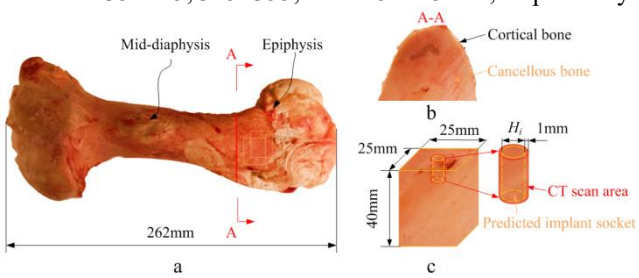

Figure 4 Preparation of bone blocks: (a) bovine femur, (b) A-A cross-section, (c) the bone blocks used in experiments and the CT scan area.

Table 1 CT value of 3 group bone blocks

Group 1	CT (HU)	Group 2	CT (HU)	Group 3	CT (HU)
A_{01}	237.60	B_{01}	354.86	C_{01}	418.48
A_{02}	241.54	B_{02}	345.35	C_{02}	419.58
A_{03}	236.42	B_{03}	352.68	C_{03}	417.99
A_{04}	237.08	B_{04}	346.42	C_{04}	422.54
A_{05}	242.13	B_{05}	348.57	C_{05}	420.26
A_{06}	239.56	B_{06}	353.63	C_{06}	421.41
A_{07}	241.69	B_{07}	349.21	C_{07}	417.69
A_{08}	235.69	B_{08}	350.96	C_{08}	423.93
A_{09}	237.72	B_{09}	354.12	C_{09}	415.34
A_{10}	240.34	B_{10}	348.56	C_{10}	419.47
A_{11}	237.32	B_{11}	350.12	C_{11}	416.95

3.2 Insertion experiments

Three groups of insertion experiments were conducted, where IS implants (IS BIS4510 and IS BIS5010, Neobiotech Co.,Ltd., Seoul, Korea) with cutting edges were used to determine bone-quality coefficients a_0~a_3 and b_0~b_3 during thread-cutting process, and ITI implants (ITI RN4510 and ITI RN5010, ITI International Team for Implantology, Basel, Switzerland) with continuous thread typed were used to determine bone-quality coefficients c_0~c_3 and d_0~d_3 during thread-forming processes. DIO SFR5010 were used to verify the established model. The geometry parameters of these implants were shown as Table 2.

Table 2 Implant parameters

Implant	Appearance	Angle (deg)	Size (mm)
IS BIS4510		β_1=1.0 β_2=17 α_1=6 α_2=30 λ=90 φ=0	L=10 D= ϕ4.5 P=0.8 h_d=0.25 w=0.08 H=ϕ4.4
IS BIS5010		β_1=1.7 β_2=17 α_1=6 α_2=30 λ=90 φ=0	L=10 D= ϕ5 P=0.8 h_d=0.25 w=0.08 H=ϕ4.9
ITI RN4210		β=0 α=30 η_1=85 η_2=10 ξ=4.74	L=10 D=ϕ4.8 P=1.25 H=ϕ4.2 w=0.1
ITI RN4810		β=0 α=30 η_1=85 η_2=10 ξ=4.74	L=10 D=ϕ4.8 P=1.25 H=ϕ4.2 w=0.1
DIO SFR5010		β_1=0 α_1=8.5 η_1=85 η_2=10 ξ=1.5 β_2=8.75 α_2=7 α_3=30 λ=90 φ=0	L_1=2.5 D_1=ϕ5.0 P_1=0.4 H_1=ϕ4.9 w_1=0.05 L_2=6.5 D_2=ϕ5 P_2=0.8 H_2=ϕ4.2 w_2=0.12

where β_1, α_1, L_1, D_1, P_1, H_1 are the parameters of apical part of implant DIO SFR5010 while β_2, α_2, α_3, L_2, D_2, P_2, H_2 the tail part of implant DIO SFR5010.

The insertion experiments, including the drilling process of implant sockets and the insertion process of implants, were conducted on the CNC machine (HAAS OM-2A, Haas Automation Inc., Oxnard, CA, USA) as shown in Figure 5. The parameters of drills, implants, and experiment setting were listed as Table. 3. To minimize the coaxiality error between the implant and corresponding implant socket, there was no interruption between the drilling and insertion processes. The high accuracy dynamometer (Kistler9119AA2, Kistler Instruments Ltd.,

London, UK, sampling rate: 1200 Hz) was used to capture the thrust forces and insertion torques during the insertion process of implants.

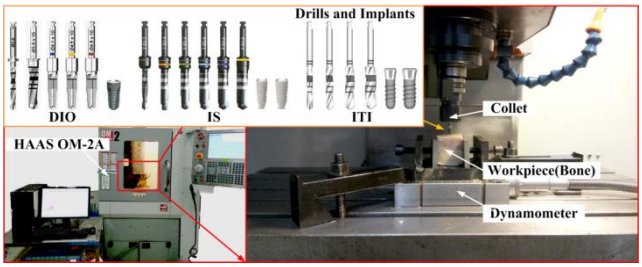

Figure 5 Preparation of bone blocks: (a) bovine femur, (b) A-A cross-section, (c) the bone blocks used in experiments and the CT scan area.

Table 3 Parameters of insertion experiments

Drills and Implants types	Bone blocks No.	Diameter d (mm)	Insertion speed ω (rpm)	Feed rate v (mm/min)
IS TSD22F	A_{01}~A_{02}; B_{01}~B_{02}; C_{01}~C_{02}	2.2	1200	10
IS TSD29F	A_{01}~A_{02}; B_{01}~B_{02}; C_{01}~C_{02}	2.9	1200	10
IS TSD34F	A_{01}~A_{02}; B_{01}~B_{02}; C_{01}~C_{02}	3.4	1200	10
IS TSD39F	A_{01}~A_{02}; B_{01}~B_{02}; C_{01}~C_{02}	3.9	1000	10
IS TSD44F	A_{01}~A_{02}; B_{01}~B_{02}; C_{01}~C_{02}	4.4	800	10
IS BIS4510	A_{01}; B_{01}; C_{01}	4.5	20	16
IS BIS4510	A_{02}; B_{02}; C_{02}	4.5	30	24
IS TSD22F	A_{03}~A_{05}; B_{03}~B_{05}; C_{03}~C_{05}	2.2	1200	10
IS TSD29F	A_{03}~A_{05}; B_{03}~B_{05}; C_{03}~C_{05}	2.9	1200	10
IS TSD34F	A_{03}~A_{05}; B_{03}~B_{05}; C_{03}~C_{05}	3.4	1200	10
IS TSD39F	A_{03}~A_{05}; B_{03}~B_{05}; C_{03}~C_{05}	3.9	1000	10
IS TSD44F	A_{03}~A_{05}; B_{03}~B_{05}; C_{03}~C_{05}	4.4	1000	10
IS TSD49F	A_{03}~A_{05}; B_{03}~B_{05}; C_{03}~C_{05}	4.9	800	10
IS BIS5010	A_{03}; B_{03}; C_{03}	5.0	20	16
IS BIS5010	A_{04}~A_{05}; B_{04}~B_{05}; C_{04}~C_{05}	5.0	30	24
ITI 044.210	A_{06}~A_{07}; B_{06}~B_{07}; C_{06}~C_{07}	2.2	800	10
ITI 044.214	A_{06}~A_{07}; B_{06}~B_{07}; C_{06}~C_{07}	2.8	600	10
ITI 044.250	A_{06}~A_{07}; B_{06}~B_{07}; C_{06}~C_{07}	3.5	500	10
ITI RN4110	A_{06}; B_{06}; C_{06}	4.1	12	15
ITI RN4110	A_{07}; B_{07}; C_{07}	4.1	15	18.75
ITI 044.210	A_{08}~A_{10}; B_{08}~B_{10}; C_{08}~C_{10}	2.2	800	10
ITI 044.214	A_{08}~A_{10}; B_{08}~B_{10}; C_{08}~C_{10}	2.8	600	10
ITI 044.250	A_{08}~A_{10}; B_{08}~B_{10}; C_{08}~C_{10}	3.5	500	10
ITI 044.254	A_{08}~A_{10}; B_{08}~B_{10}; C_{08}~C_{10}	4.2	400	10
ITI RN4810	A_{08}; B_{08}; C_{08}	4.8	12	15
ITI RN4810	A_{09}~A_{10}; B_{09}~B_{10}; C_{09}~C_{10}	4.8	15	18.75
DIO DHI 2010SM	A_{11}~A_{12}; B_{11}~B_{12}; C_{11}~C_{12}	2.0	1000	10
DIO SDS 2710M	A_{11}~A_{12}; B_{11}~B_{12}; C_{11}~C_{12}	3.5	1000	10
DIO DTS 4110M	A_{11}~A_{12}; B_{11}~B_{12}; C_{11}~C_{12}	4.0	1000	10
DIO DTS 4510M	A_{11}~A_{12}; B_{11}~B_{12}; C_{11}~C_{12}	4.4	1000	10
DIO DTI 5010SM	A_{11}~A_{12}; B_{11}~B_{12}; C_{11}~C_{12}	4.9	800	10
DIO SFR5010	A_{11}~A_{12}; B_{11}~B_{12}; C_{11}~C_{12}	5.0	15	12

3.3 Bone-quality coefficients

The results of thrust forces F_{thr_i} and insertion torques of IS and ITI implants were presented as follows:

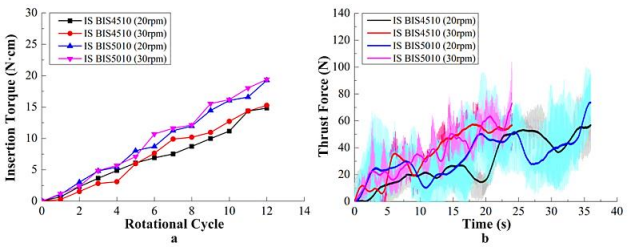

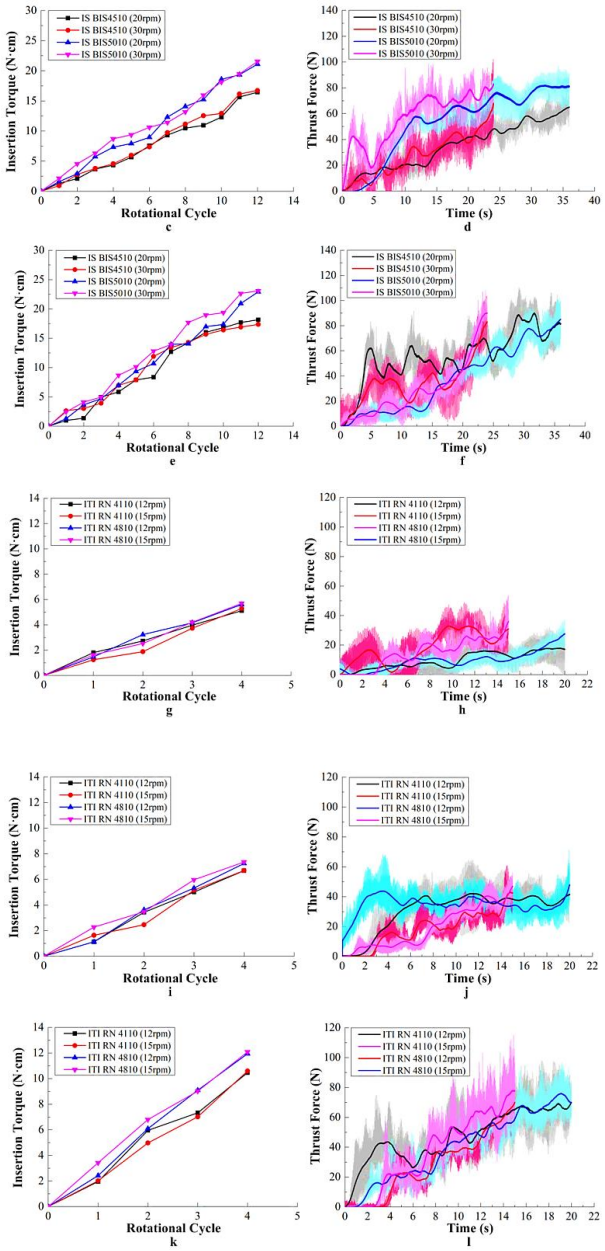

Figure 6 The insertion torques and thrust forces obtained by insertion experiments: (a)~(f) data of IS implants, (a) and (b), (c) and (d), (e) and (f) were insertion torques and thrust forces of 235~245Hu, 345~355 Hu and 415~425 Hu, respectively; (g)~(l) data of ITI implants, (g) and (h), (i) and (j), (k) and (l) were insertion torques and thrust forces of 235~245Hu, 345~355 Hu and 415~425 Hu, respectively.

The peak torque and thrust force were used to determine the bone-quality coefficients for thread-cutting and thread-forming processes. The obtained bone-quality coefficients were listed in Tables 4 and 5.

Table 4 Bone-quality coefficients for thread-cutting

Group	a_0	a_1	a_2	a_3	b_0	b_1	b_2	b_3
1	14.5610	0.1662	0.4429	0.0332	12.9085	0.0176	0.1746	0.0033
2	16.6887	0.3697	0.7743	0.0662	13.2065	0.0191	0.1768	0
3	58.1214	4.8069	8.1865	0.8613	52.8202	4.4348	7.2909	0.7947

Table 5 **Bone-quality coefficients for thread-forming**

Group	c_0	c_1	c_2	c_3	d_0	d_1	d_2	d_3
1	22.4146	0.0618	0.1517	0	21.2106	0.0618	0.1517	0
2	27.3438	0.5678	0.8236	0.0716	26.1398	0.5678	0.8236	0.0716
3	60.4041	3.8712	6.8643	0.6841	59.2001	3.8712	6.8643	0.6841

It was observed that the bone-quality coefficients a_0~a_3, b_0~b_3, c_0~c_3 and d_0~d_3 were different in 3 group with CT value of 235~245, 345~355 and 415~425 HU, which is the great explanation for the effects of bone quality.

3.4 Validation of mechanical model

Substituting obtained bone-quality coefficients into the established model, the predicted insertion torque and measured insertion torque were shown in Figure 7 and Table 6.

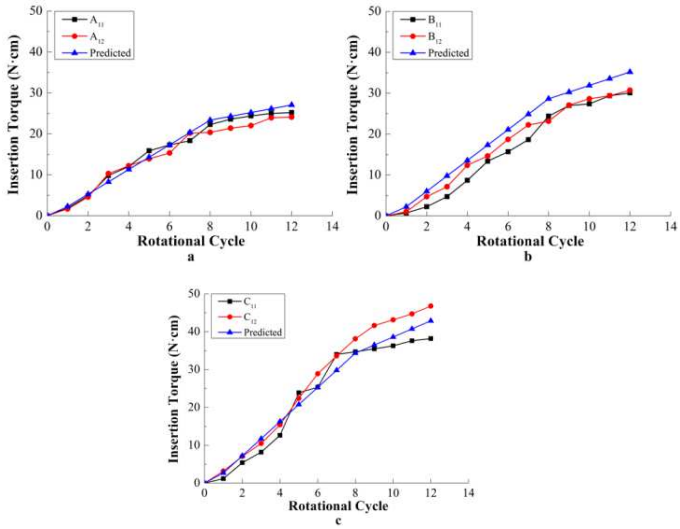

Figure 7 Insertion torques obtained by the mechanical model and experiments

Table 6 Comparison of averaged insertion torques from experiments and predictions

Thread number	Group 1			Group 2			Group 3		
	Measured (N·cm)		Pred (N·cm)	Measured (N·cm)		Pred (N·cm)	Measured (N·cm)		Pred (N·cm)
1	1.899	1.669	2.256	0.693	1.036	2.244	1.167	3.158	2.693
2	4.872	4.559	5.270	2.237	4.693	6.012	5.394	7.061	7.214
3	9.805	10.272	8.284	4.693	7.125	9.779	8.171	10.475	11.735
4	12.050	12.197	11.298	8.693	12.362	13.547	12.617	15.392	16.256
5	15.874	13.893	14.312	13.369	14.639	17.314	23.872	22.389	20.777
6	17.274	15.325	17.326	15.693	18.693	21.082	25.349	28.869	25.298
7	18.326	20.186	20.340	18.639	22.237	24.849	33.995	33.612	29.819
8	22.264	20.362	23.354	24.363	23.140	28.617	34.693	38.118	34.34
9	23.592	21.369	24.279	26.964	27.063	30.256	35.460	41.636	36.471
10	24.362	22.012	25.206	27.365	28.634	31.895	36.256	43.124	38.602
11	24.982	23.937	26.132	29.369	29.363	33.534	37.596	44.691	40.733
12	25.193	24.102	27.058	30.069	31.693	35.174	38.172	46.786	42.864
error	7.4%	12.3%	0	16.9%	10.9%	0	12.4%	8.4%	0

As shown in Figure 7, the variations of material properties of bone blocks brought a significant fluctuation of the initial insertion torques obtained by experiments. But the trends and predicted peak insertion torques by mechanical models agreed well with that acquired by insertion experiments. The relative errors were calculated as follows.

$$\frac{T_{pred}-T_{measured}}{T_{measured}}\times 100\% \tag{30}$$

4 Conclusions

In this present research, a mechanical model was established for predicting insertion torque of dental implant. The effect of bone quality, the surgical method and the implant geometry were explained by the model parameters: *a*) bone-quality coefficients, *b*) insertion speed, and *c*) radial engagement h_i, chip load A and implant diameter r_i, respectively. The more specific conclusions can be drawn as follows:

(1) The bone-quality coefficients were determined by bone CT value and different in implants with or without cutting edges. The reasonable explanation for this phenomenon may be the bone quality depended on not only bone density, i.e., bone CT value, but also the microstructure of trabecular bone.

(2) The error of this mechanical model may result from the effects of local anisotropy of cancellous bone, which were ignored in the present research.

(3) The established mechanical model can help clinicians to make accurate assessment whether the implants and surgical methods are reasonable for individual. Comparing to the fitting formula, this method could avoid plenty of experiments caused by changing implants and surgical method.

5 Declaration

Acknowledgements

The authors sincerely thanks to Professor Feng Jiang of Huaqiao University for his kindness help and critical discussion during experiment preparation.

Funding

Supported by Science and Technology Development Program of Shandong Province (Grant No. 2015GGE27218), and Taishan Scholars Program of Shandong Province (Grant No. ts201712002).

Availability of data and materials

The datasets supporting the conclusions of this article are included within the article.

Authors' contributions

The author' contributions are as follows: Song Zhang was in charge of the whole trial; Luli Li wrote the manuscript; Luli Li, Quhao Li, Cuirong Bian, Airong Zhang assisted with

sampling and laboratory analyses.

Competing interests

The authors declare no competing financial interests.

Consent for publication

Not applicable

Ethics approval and consent to participate

Not applicable

References

[1] Irinakis T, Wiebe C. Initial Torque Stability of a New Bone Condensing Dental Implant. A Cohort Study of 140 Consecutively Placed Implants. J Oral Implantol,35 (2009), pp.277-282.

[2] Nappo A, Rengo C, Pantaleo G, et al. Influence of Implant Dimensions and Position on Implant Stability: A Prospective Clinical Study in Maxilla Using Resonance Frequency Analysis[J]. Applied Science-Basel, 2019, 9(5): 43-54.

[3] Aglietta M, Siciliano V, Zwahlen M, et al. A systematic review of the survival and complication rates of implant supported fixed dental prostheses with cantilever extensions after an observation period of at least 5 years[J]. Clinical Oral Implants Research, 2009, 20(5): 441-451.

[4] Rizkallah N, Fischer S, Kraut R A. Correlation between insertion torque and survival rates in immediately loaded implants in the maxilla: a retrospective study[J]. Implant Dentistry, 2013, 22(3):250-254.

[5] Lim S A, Cha J Y, Hwang C J. Insertion torque of orthodontic miniscrews according to changes in shape, diameter and length.[J]. Angle Orthodontist, 2008, 75(2):234-240.

[6] Freitas A C, Bonfante E A, Giro G, et al. The effect of implant design on insertion torque and immediate micromotion[J]. Clinical Oral Implants Research, 2015, 23(1):113-118.

[7] Nikellis I, Levi P, Nicolopoulos M, et al. Immediate Loading of 190 Endosseous Dental Implants: A Prospective Observational Study of 40 Patient Treatments with up to 2-year Data[J]. International Journal of Oral & Maxillofacial Implants, 2004, 19(1): 116-123.

[8] Akkocaoglu M, Cehreli MC, Tekdemir I, Comert A, Güzel E, Deviren AD, Akca K. Primary Stability of Simultaneously Placed Dental Implants in Extraoral Donor Graft Sites: A Human Cadaver Study. Journal of Oral & Maxillofacial Surgery Official Journal of the American Association of Oral & Maxillofacial Surgeon, 65 (2007) pp.400-407.

[9] Trisi P, Perfetti G, Baldoni E, Berardi D, Scogna G. Implant micromotion is related to peak insertion torque and bone density. Clin Oral Implants Res, 20 (2010), pp.467-471.

[10] Turkyilmaz I, Tumer C, Ozbek EN, Tözüm TF. Relations between the bone density values from computerized tomography, and implant stability parameters: a clinical study of 230 regular platform implants. J Clin Periodontol,34 (2010), pp.716-722.

[11] Keaveny TM, Morgan EF, Niebur GL, Yeh OC. Biomechanics of Trabecular Bone. Annu Rev Biomed Eng, 3(2001), pp.307-333.

[12] Wilmes B, Su Y, Drescher D.Insertion Angle Impact on Primary Stability of Orthodontic Mini-Implants. Angle Orthod,78 (2008), pp.1065-1070.

[13] Patel PSD, Shepherd DET, Hukins DWL. The effect of screw insertion angle and thread type on the pullout strength of bone screws in normal and osteoporotic cancellous bone models. Med Eng Phys,32 (2010) pp.822-828.

[14] Wilmes B, Drescher D. Impact of bone quality, implant type, and implantation site preparation on insertion torques of mini-implants used for orthodontic anchorage. International Journal of Oral & Maxillofacial Surgery,40 (2011) pp.697-703.

[15] Sakoh J, Wahlmann U, Stender E, Nat R, Al-Nawas B, Wagner W. Primary stability of a conical implant and a hybrid, cylindrical screw-type implant in vitro. Int J Oral Max Impl, (2006), pp.560-566.

[16] Elias C N, Rocha F A, Nascimento A L, et al. Influence of implant shape, surface morphology, surgical technique and bone quality on the primary stability of dental implants[J]. Journal of the mechanical behavior of biomedical materials, 2012, 16(1): 169-180.

[17] Shalabi MM, Wolke JGC, Jansen JA. The effects of implant surface roughness and surgical technique on implant fixation in an in vitro model. Clin Oral Implan Res,17 (2010), pp.172-178.

[18] Makary C, Rebaudi A, Sammartino G, et al. Implant Primary Stability Determined by Resonance Frequency Analysis: Correlation with Insertion Torque, Histologic Bone Volume, and Torsional Stability at 6 Weeks[J]. Implant Dentistry, 2012, 21(6): 474-480.

[19] Beer A, Gahleitner A, Holm A, Tschabitscher M, Homolka P. Correlation of insertion torques with bone mineral density from dental quantitative CT in the mandible. Clin Oral Implants Res,14 (2010), pp.616-620.

[20] Ozan O, Orhan K, Turkyilmaz I. Correlation Between Bone Density and Angular Deviation of Implants Placed Using CT-Generated Surgical Guides. J Craniofac Surg, 22 (2011), pp.1755-1761.

[21] Lee JH, Park J, Lee J, Lee HS. The Correlation between Insertion Torque of Pedicle Screws with Bone Mineral Density Values in Posterior Lumbar Pedicle Screw Fixation. Spine J,11(2011), pp.S145-S146.

[22] Agapiou JS. Evaluation of the Effect of High Speed Machining on Tapping. Journal of Engineering for Industry,116 (1994), pp.457-462.

[23] Fromentin G, Poulachon G, Moisan A, Julien B, Giessler J. Precision and surface integrity of threads obtained by form tapping. CIRP Annals - Manufacturing Technology,54 (2005), pp.519-522.

[24] Cao T, Sutherland JW. Investigation of thread tapping load characteristics through mechanistics modeling and experimentation. Int J Mach Tool Manu,42 (2002), pp.1527-1538.

[25] Dogra APS, Kapoor SG, DeVor RE. Mechanistic Model for Tapping Process With Emphasis on Process Faults and Hole Geometry. Journal of Manufacturing Science & Engineering,124 (2002), pp.18.

[26] Lee JE, Gozen BA, Ozdoganlar OB. Modeling and experimentation of bone drilling forces. J Biomech,45(2012), pp.1076-1083.

[27] Jiang F, Zhang T, Yan L. Analytical model of milling forces based on time-variant sculptured shear surface. Int J Mech Sci,115 (2016) pp.190-201.

[28] Moufki A, Dudzinski D, Molinari A, Rausch M. Thermoviscoplastic modelling of oblique cutting: Forces and chip flow predictions. Int J Mech Sci,42 (2000), pp.1205-1232.

[29] Liu XW, Cheng K, Webb D, Longstaff AP, Widiyarto MH. Improved dynamic cutting force model in peripheral milling. Part II: experimental verification and prediction. Int J Adv Manuf Tech,24 (2004), pp.794-805.

[30] Chowdhary S, Devor RE, Kapoor SG. Modeling Forces Including Elastic Recovery for Internal Thread Forming. Journal of Manufacturing Science & Engineering,125 (2015), pp.681-688.

Biographical notes

Lu-Li Li, received her master degree from Shandong University, China, in 2019. Her research interests include dental implant and bone mechanics.
E-mail: sdbolll@163.com

Song Zhang, received his PhD degree from *Shandong University, China*, in 2004. He is currently a professor and doctoral supervisor at *School of Mechanical Engineering, Shandong University*, China. His research fields are fundamental mechanism of high-efficiency cutting and machined surface integrity, biomechanics, and so on.

Tel: +86-531-88392746; E-mail: zhangsong@sdu.edu.cn

Qu-Hao Li, received his PhD degree from *Dalian University of Technology, China*, in 2017. He is currently a lecture at *School of*

Mechanical Engineering, Shandong University, China. He His research interests include computational solid mechanics, numerical simulation.
E-mail: quhaoli@sdu.edu.cn

Cui-Rong Bian, received her M.M. degree from S*handong University, China*, in 2004. She is currently a Professor and a chief physician at Department of Prosthodontics, Qilu Hospital of Shandong University. Her research fields are fixed porcelain repair, reconstruction of maxillofacial bone defects, implant surgery and design, design and fabrication of denture, and so on.
E-mail: cuirong_b88@163.com

Ai-Rong Zhang, received her PhD degree from *Shandong University, China*, in 2020. Her research interests include bone mechanics, dental implant and numerical simulation of bone tissue.
E-mail: zhangar_ll@163.com

Figures

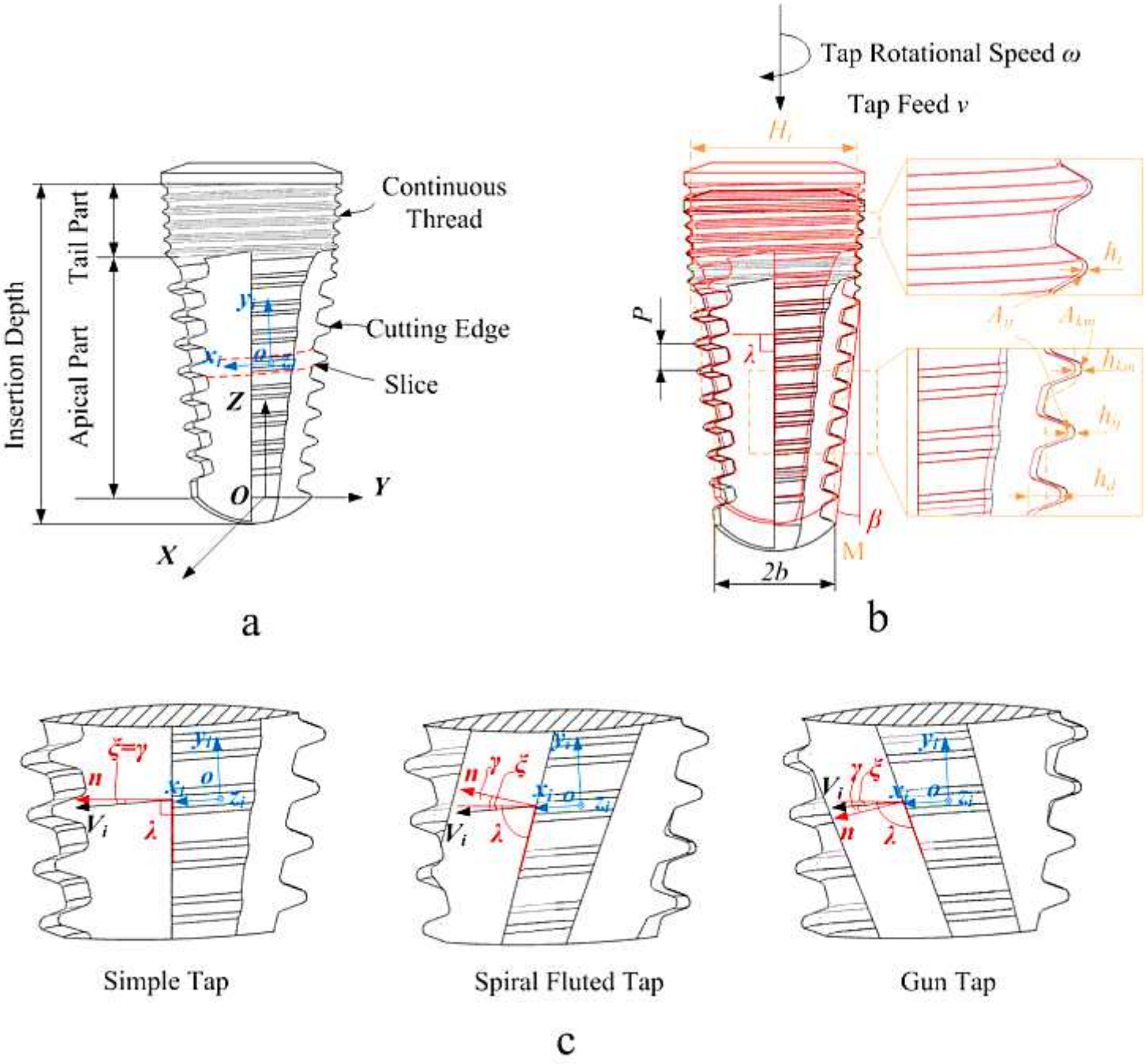

Figure 1

DIO SFR5010 and its insertion process: (a) the geometry of DIO SFR5010 and two coordinate systems, (b) geometric parameters of DIO SFR5010 and the insertion process: the initial position was in red and the position of one rotation cycle was in black, (c) the relationship of angle parameters γ, ξ and λ.

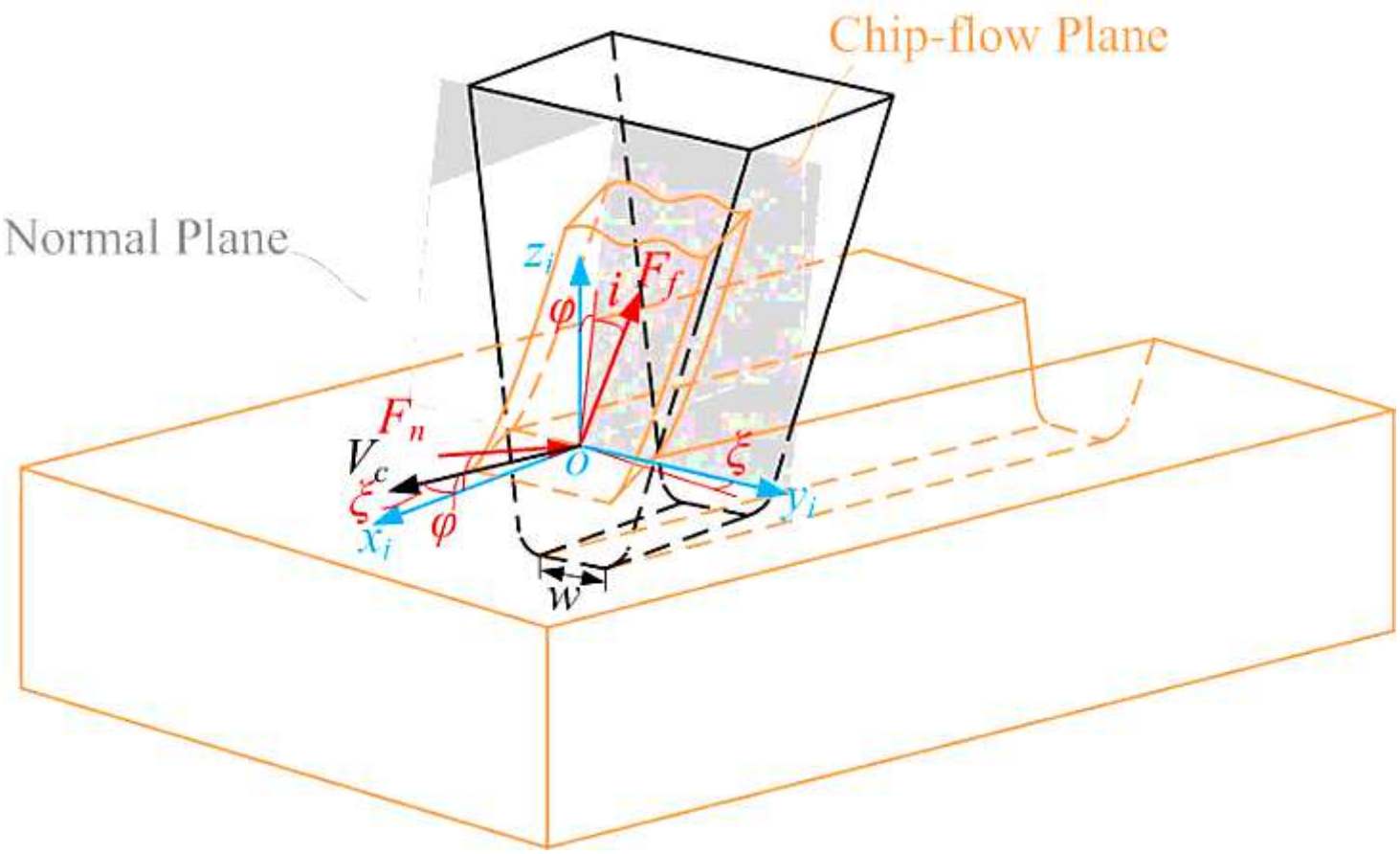

Figure 2

The oblique cutting process

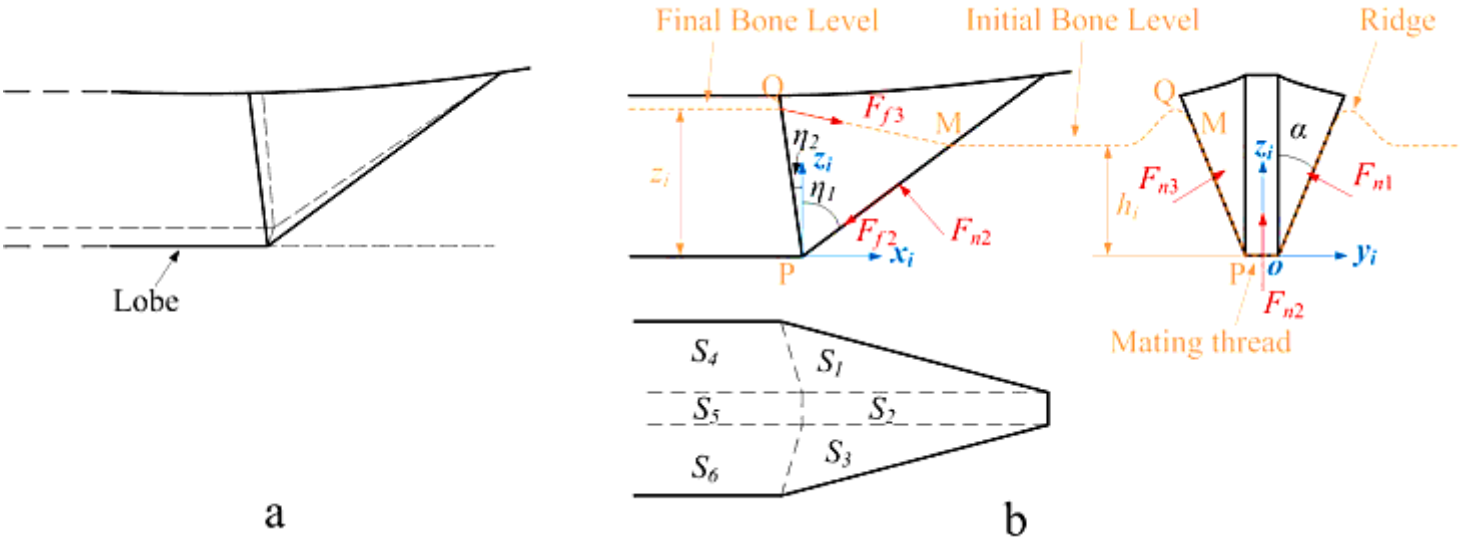

Figure 3

A typical form tap tooth: (a) the schematic diagram of form tap tooth; (b) three views of ith tooth.

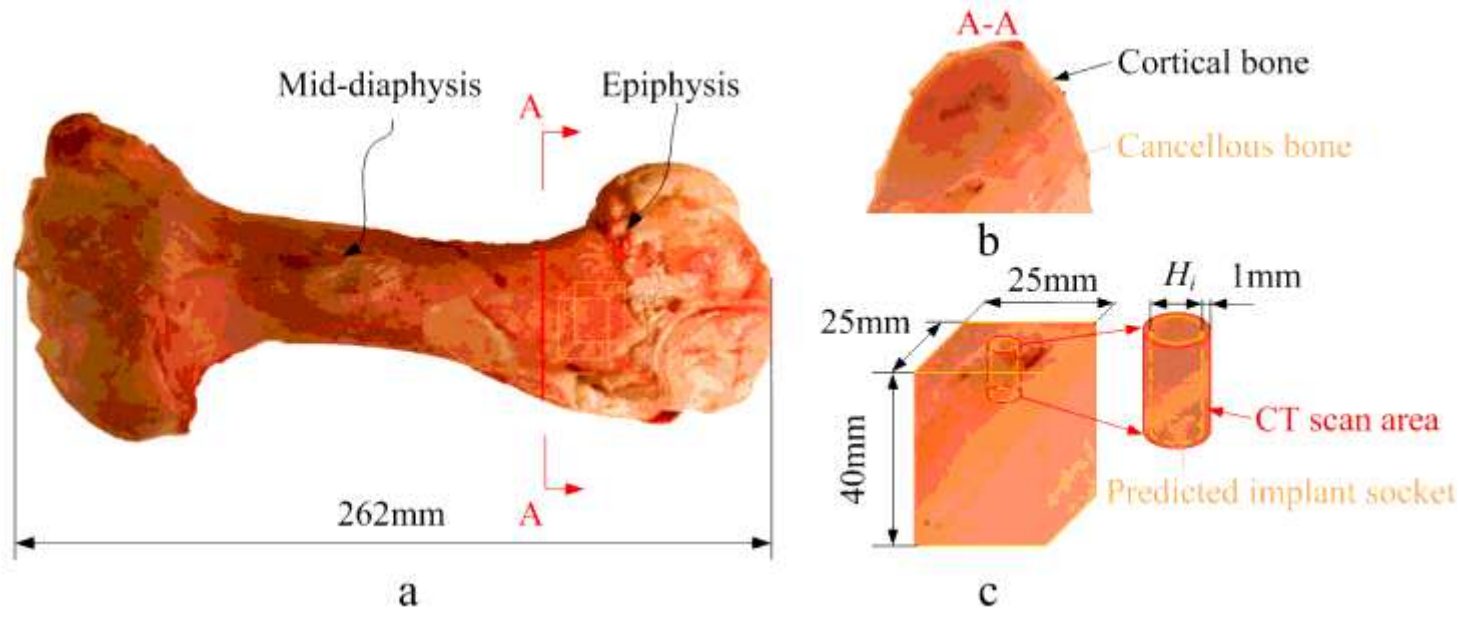

Figure 4

Preparation of bone blocks: (a) bovine femur, (b) A-A cross-section, (c) the bone blocks used in experiments and the CT scan area.

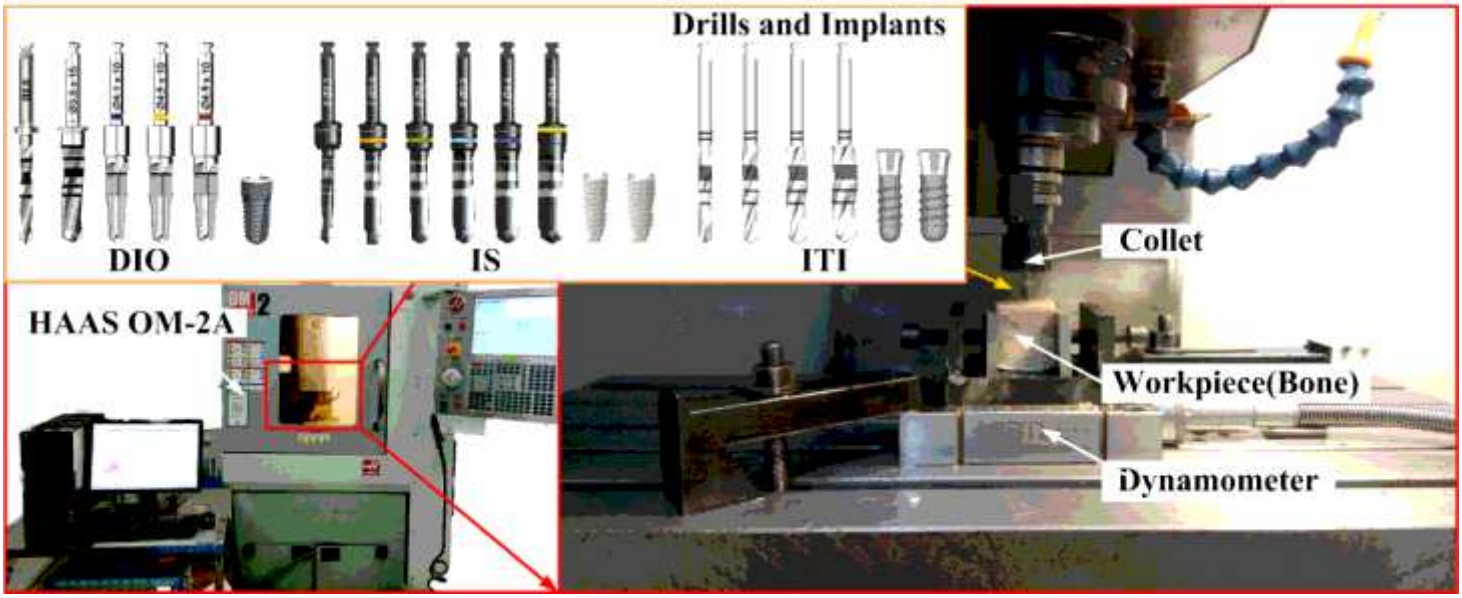

Figure 5

Preparation of bone blocks: (a) bovine femur, (b) A-A cross-section, (c) the bone blocks used in experiments and the CT scan area.

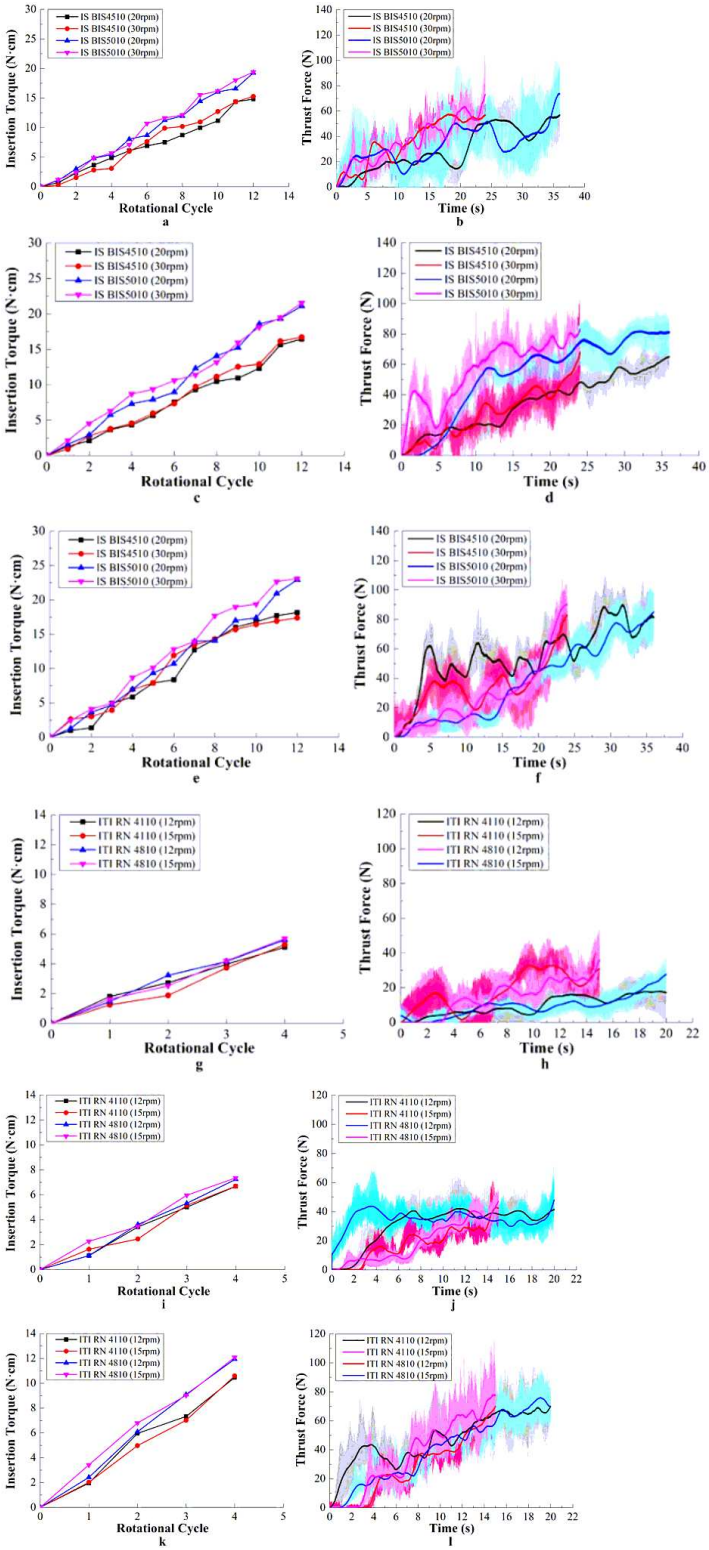

Figure 6

The insertion torques and thrust forces obtained by insertion experiments: (a)~(f) data of IS implants, (a) and (b), (c) and (d), (e) and (f) were insertion torques and thrust forces of 235~245Hu, 345~355 Hu and 415~425 Hu, respectively; (g)~(l) data of ITI implants, (g) and (h), (i) and (j), (k) and (l) were insertion torques and thrust forces of 235~245Hu, 345~355 Hu and 415~425 Hu, respectively.

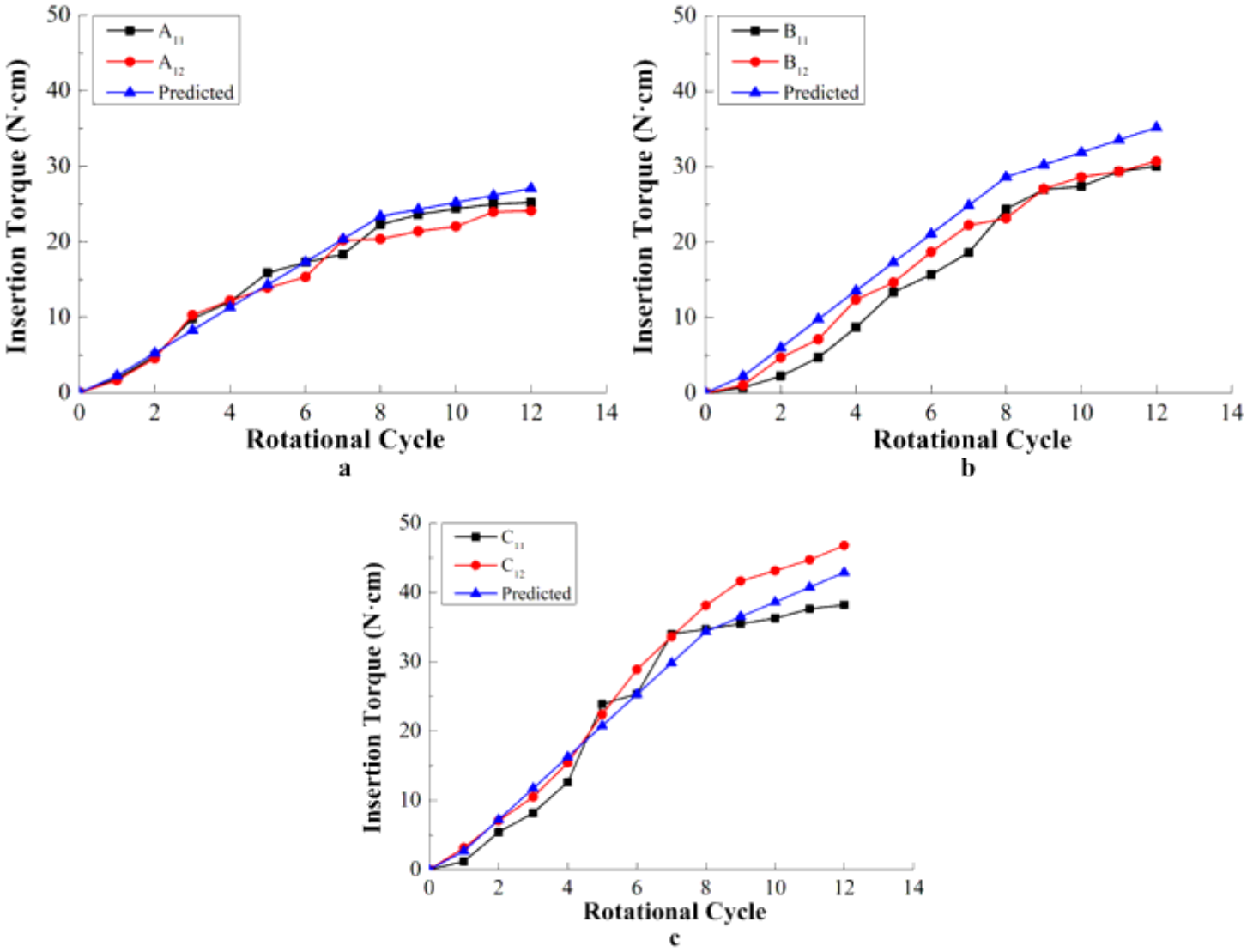

Figure 7

Insertion torques obtained by the mechanical model and experiments